Journal of Catalysis 265 (2009) 43–53

Contents lists available at ScienceDirect

Journal of Catalysis

journal homepage: www.elsevier.com/locate/jcat

Mo-containing tetragonal tungsten bronzes. The influence of tellurium on catalytic behaviour in selective oxidation of propene

P. Botella [a], E. García-González [b], B. Solsona [a,c], E. Rodríguez-Castellón [d], J.M. González-Calbet [b], J.M. López Nieto [a,*]

[a] Instituto de Tecnología Química, UPV-CSIC, Avenida de los Naranjos s/n, 46022 Valencia, Spain
[b] Dpto. Química Inorgánica, Facultad de Ciencias Químicas, Universidad Complutense Madrid, 28040 Madrid, Spain
[c] Departamento de Ingeniería Química, Universidad de Valencia, Dr. Moliner 50, 46100 Burjassot, Spain
[d] Dpto. Química Inorgánica, Facultad de Ciencias, Universidad de Málaga, 29071 Málaga, Spain

ARTICLE INFO

Article history:
Received 5 January 2009
Revised 14 April 2009
Accepted 14 April 2009
Available online 12 May 2009

Keywords:
Tetragonal tungsten bronze (TTB) structure
Multicomponent mixed metal oxides
Mo–Nb–V–P–Te
Partial oxidation of hydrocarbons
Propene
Acrolein
Acrylic acid

ABSTRACT

Te-free and Te-containing multicomponent Mo-based catalysts presenting tetragonal tungsten bronze (TTB) structure have been prepared, characterized and tested for the selective oxidation of propene. The catalysts were prepared hydrothermally and heat treated at 700 °C. The structural characterization performed by means of XRD, FTIR, SAED and HRTEM confirms the incorporation of tellurium to the TTB structural framework and shows that its presence does not modify in essence the crystalline structure. However, the incorporation of Te strongly modifies the catalytic performance, and the highest yield to acrolein has been achieved on catalysts with Te/Mo atomic ratios in bulk of 0.03. The XPS results indicate a Te enrichment on the catalyst surface in all the studied catalysts, suggesting important modifications of the surface in Te-containing catalysts. In this way, tellurium atoms seem to be a key element in the selective oxidative activation of olefin.

1. Introduction

Mo-based bronzes have been proposed as constituents of important catalytic systems active and selective for the (amm)oxidation of propane to acrylonitrile/acrylic acid [1–3] or in the oxidative dehydrogenation of ethane to ethylene [4,5], which are processes of high interest from an industrial point of view. These materials are characterized by the presence of at least two crystalline phases [1–14]: (i) the orthorhombic $X_2M_{20}O_{57}$ (M = Mo, V, Nb; X = Te, Sb) isostructural with $Cs_x(Nb,W)_5O_{14}$ [10–12] and (ii) the pseudo-orthorhombic $X_{0.33}MO_{3.33}$ (M = Mo, V, Nb; X = Te, Sb) HTB (hexagonal tungsten bronze)-type oxide [12,13]. Moreover, the chemical composition and the catalytic behaviour of these crystalline phases strongly depend on the catalyst preparation procedure [14].

The synthesis of Mo–V–Y–O (Y = Te, Sb, Al, Fe, Cr, Ti), which are active catalysts in selective oxidation of short chain alkanes, is of special interest. Both Nb-free and Nb-containing mixed oxides are generally obtained from ammonium heptamolybdate as well as Anderson-type heteropolymolybdates, although the Te-precursor compound and composition are key factors for the synthesis of active and selective catalysts [6–11].

It has been recently proposed that Nb–V–X–Y–O mixed oxides (X = Mo, W; Y = Te, Sb, Bi) that are prepared hydrothermally from Keggin-type heteropolyoxometallates and heated in oxygen-free atmosphere transform into tetragonal tungsten bronze-type phase and are active and selective in partial oxidation of olefins [15,16].

In this context, the crystal chemistry of the binary system Nb_2O_5/WO_3 has been extensively studied, and significant structural variations are found by changing the oxygen/metal (O/M) ratio. Structure types derived from the tetragonal tungsten bronze, where MO_6 octahedra are corner linked to give five-membered rings arranged around square tunnels, are formed in the composition range $2.67 < O/M < 2.9$ [17,18] (see Fig. 1). Compositional variations can be accommodated by filling of a certain portion of the pentagonal tunnels with metal–oxygen chains (preferentially by niobium atoms) leading to a pentagonal bipyramidal coordination of the corresponding metal cation. The MO_7 polyhedra so formed share the equatorial edges with five octahedra. Infinite strings of these units connected along the perpendicular direction form the so-called pentagonal columns (PCs). The systematic occupation of four of twelve pentagonal tunnels gives rise to the threefold TTB superstructure of $Nb_8W_9O_{47}$ (the so-called 4:9 phase, O/M = 2.76), which is thermodynamically favoured in the

* Corresponding author. Fax: +34 963877809.
E-mail address: jmlopez@itq.upv.es (J.M. López Nieto).

0021-9517/$ - see front matter © 2009 Elsevier Inc. All rights reserved.
doi:10.1016/j.jcat.2009.04.008

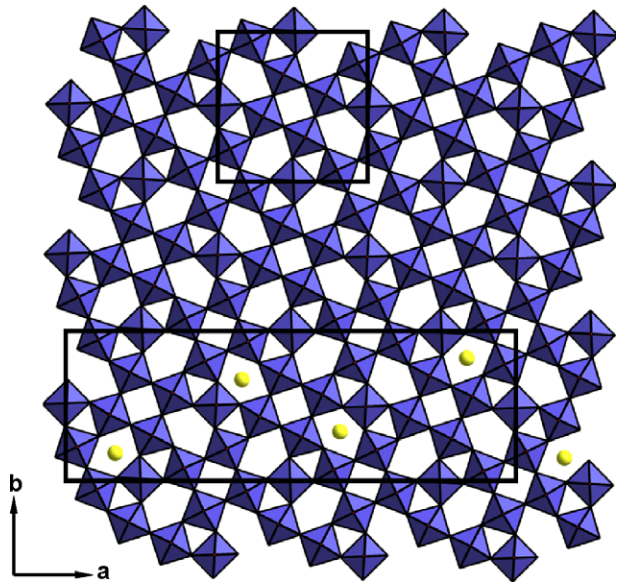

Fig. 1. Schematic representation of the structural skeleton of the TTB-type structure projected on the *ab* plane. Blue polyhedra correspond to the [001] projected MO6 octahedra (M = Mo, Nb, V) of the TTB framework. The ordered occupation of the pentagonal tunnels following the pattern resembled by the yellow spheres gives rise to the threefold superstructure whose unit cell has been outlined in the figure together with the basic structure.

above-mentioned composition range [19]. The corresponding unit cell has been outlined in comparison with that of the TTB substructure in Fig. 1. For compositions different that O/M = 2.76, short-range ordered structures are formed related to the distribution of filled PC elements [20–24].

In the present contribution, we report the catalytic behaviour for propene oxidation of Mo–Nb–V TTB-type oxides prepared hydrothermally from Keggin-type heteropolyoxometallates. The microstructural aspects of the obtained oxides are analyzed taking into account the parallelism with the Nb_2O_5/WO_3 system. The catalysts' activity dramatically changes with the incorporation of Te atoms in the structural framework. The nature of the active and selective sites, the importance of the cationic distribution and the role of the catalyst structure on the catalytic performance hill be discussed.

2. Experimental

2.1. Catalyst synthesis

The catalysts have been prepared by hydrothermal synthesis from gels containing $H_3PMo_{12}O_{40}$(Aldrich), vanadyl sulphate (Aldrich), niobium oxalate (CBMM) and telluric acid (Aldrich) [15]. The resulting gels with a Mo/Nb/V/P/Te atomic ratio of 1/0.17/0.20/0.08/*x* (*x* = 0 to 0.24) were incorporated to a Teflon-lined, stainless steel autoclave and heated at 175 °C for 48 h. The solid so obtained was filtered off, washed and dried at 80 °C for 16 h. Finally, the samples were heated at 700 °C in flowing N_2 for 2 h. For calcination temperatures below 700 °C, pseudocrystalline materials were always obtained (see Section 3). Catalysts were named as C*n*-T*x*, where *n* is related to the Te/Mo atomic ratio in the synthesis gel and *x* is related to the heating temperature (i.e. C1-T7 corresponds to a sample with a Te/Mo atomic ratio of 0.01 calcined at 700 °C). A Te-free sample (C0-T7) is also included. The main characteristics of the catalysts are summarized in Table 1.

In order to compare the catalytic activity, a MoVTeNbO mixed oxide with the so-called M2 phase, i.e. a pseudo-orthorhombic $Te_{0.33}MO_{3.33}$ (with M = Mo, V and Nb), is prepared according to the catalyst preparation procedure reported previously [25]. This catalyst is named as CAT-M2.

2.2. Catalyst characterization

Bulk composition of both hydrothermal and heated samples was determined by inductive coupled plasma (ICP). Average chemical composition of the heated samples was also determined by X-ray energy dispersive spectroscopy (XEDS) analysis performed on a JEOL JSM 6300 scanning electron microscope equipped with a LINK ISIS system. The quantitative analysis was performed with the SEMQUANT program, which introduces the ZAF correction.

Powder X-ray diffraction (XRD) patterns were collected using an Enraf Nonius FR590 sealed tube diffractometer, with a monochromatic $CuK_{\alpha 1}$ source operating at 40 kV and 30 mA. XRD patterns were calibrated against a silicon standard and phases were identified by matching experimental patterns to the JCPDS powder diffraction file (reference number 80-02136) of $Ba_3Nb_5O_{15}$.

Samples for transmission electron microscopy were ultrasonically dispersed in *n*-butanol and were transferred to carbon-coated copper grids. Selected area electron diffraction (SAED) and high-resolution transmission electron microscopy (HRTEM) were performed on a JEOL JEM300FEG electron microscope. The microscope is equipped with an ISIS 300 X-ray microanalysis system (Oxford Instruments) with a LINK "Pentafet" detector which has been used to analyze the chemical composition of the crystal phases by means of crystal by crystal XEDS microanalysis.

Infrared spectra were recorded at room temperature in the 300 to 3900 cm^{-1} region with a Nicolet 205xB spectrophotometer, equipped with a Data Station, at a spectral resolution of 1 cm^{-1} and accumulations of 128 scans.

X-ray photoelectron spectra were collected using a Physical Electronics PHI 5700 spectrometer with a non monochromatic MgKα radiation (300 W, 15 kV, 1253.6 eV) for the analysis of photoelectronic signals of C 1*s*, O 1*s*, Mo 3*d*, Nb 3*d*, V 2*p*, P 2*p* and Te 3*d* and with a multi-channel detector. Spectra of powder samples were recorded with the constant pass energy values at 29.35 eV, using a 720 μm diameter analysis area. Under these conditions, the Au $4f_{7/2}$ line was recorded with 1.16 eV FWHM at a binding energy of 84.0 eV. The spectrometer energy scale was calibrated by using the Cu $2p_{3/2}$, Ag $3d_{5/2}$ and Au $4f_{7/2}$ photoelectron lines at 932.7, 368.3 and 84.0 eV, respectively. During data processing of the XPS spectra, binding energy values were referenced to the C 1*s* peak (284.8 eV) from the adventitious contamination layer. The PHI ACCESS ESCA-V6.0 F software package was used for acquisition and data analysis. A Shirley-type background was subtracted from the signals. Recorded spectra were always fitted using Gauss–Lorentz curves, in order to determine the binding energy of the different element core levels more accurately. The error in BE was estimated to be ca. 0.1 eV. Short acquisition time of 10 min was used to examine C 1*s* and V 2*p* regions in order to avoid, as much as possible, photoreduction of V^{5+} species. Satellite subtraction was always performed to study the V 2*p* region.

Diffuse Reflectance (DR) UV–vis spectra were collected on a Cary 5 equipped with a 'Praying Mantis' attachment from Harric. Reference compounds, such as V_2O_5, MgV_2O_6, $VOSO_4$, TeO_2, MoO_3 and $TeMo_5O_{16}$, have been used [26].

The surface areas of the catalysts were measured on a Micromeritics ASAP 2000 instrument by adsorption of krypton.

2.3. Catalytic experiments

Catalytic tests in propene oxidation have been undertaken using a fixed-bed laboratory microreactor, at atmospheric pressure, in the temperature range 360 to 380 °C. The feed corresponds to a mixture

Table 1
Characteristics of Mo-based catalyst.

Catalyst	Te/Mo ratio (gel)[a]	Temperature (°C)[b]	Mo/Nb/V/P/Te atomic ratio		
			Bulk[c]	XPS	Crystal by Crystal [d]
C0-T7	0	700	1/0.48/0.16/0.11/0	1/0.42/0.13/0.07/0	1/0.52/0.1/0.05/0
C1-T7	0.01	700	1/0.39/0.19/0.08/0.01	1/0.40/0.19/0.06/0.04	1/0.55/012/0.08/0.04
C2-T7	0.02	700	1/0.39/0.19/0.08/0.02	nd	
C3-T7	0.03	700	1/0.39/0.19/0.08/0.03	nd	
C4-T7	0.04	700	1/0.42/0.16/0.08/0.15	1/0.22/0.13/0.05/0.41	
C8-T7	0.08	700	1/0.44/0.15/0.08/0.23	1/0.28/0.14/0.05/0.66	1/0.54/013/0.08/0.04
C17-T7	0.17	700	1/0.44/0.15/0.08/0.40	nd	1/0.53/011/0.08/0.05
C8-T5	0.08	500	1/0.44/0.15/0.08/0.27	nd	
C8-T6	0.08	600	1/0.44/0.15/0.08/0.27	nd	
CAT-M2[e]	0.58	600	1/0.18/0.8/0/0.58	nd	

[a] Te/Mo ratio in the synthesis gel in Mo/Nb/V/P/Te ratio of 1/0.17/0.20/0.08/x (x = 0 to 0.17).
[b] Calcination temperature.
[c] Atomic composition was done by XEDS.
[d] As determined by microanalysis XEDS nd = not determined.
[e] Data from Ref. [25].

consisting of $C_3H_6/O_2/He/H_2O$ (with a molar ratio of 1.5/6.0/77.5/15) and a total flow of 25 to 50 ml min^{-1}. Reactants and reaction products were analyzed online by gas chromatography using two different columns: (i) Molecular Sieve 5A and Porapak Q [14]. The carbon balance was estimated with an accuracy of ±3%.

3. Results and discussion

3.1. Catalyst characterization

Table 1 presents a summary of the characteristics of the catalysts. After heating, dark-brown to purple powders with very low surface area (about 5.0 $m^2 g^{-1}$) were obtained.

Fig. 2 shows the powder XRD patterns of representative catalysts. In the case of samples heated at 700 °C (diagrams a–d), diffraction patterns can be assigned to the unit cell of the TTB structure (JCPDS file No. 80-02136) with approximate parameters 12.1 × 12.1 × 4 Å. Although diffraction maxima match with those of a basic TTB unit cell, the relative intensities are closer to the relative intensity of reflections in the ordered $M_{17}O_{47}$ phase. However, superstructure reflections appearing in the low angle zone ($6° < 2\theta < 12°$) are not visible, indicating that certain extra order in respect to the TTB must occur but only in short extension. The XRD patterns of Te-free and Te-containing samples calcined at 500 °C and 600 °C have also been included for comparison (patterns a_1, a_2, c_1 and c_2). It is important to mention that no appreciable differences are observed in the unit cell parameters of Te-free and Te-containing samples. This is not surprising since tellurium atoms, when present, must be located in the tunnels of the structure and, also, the TTB framework is quite rigid and presents a constant chemical composition for all samples (see Table 1). Pseudocrystalline materials were always obtained for samples

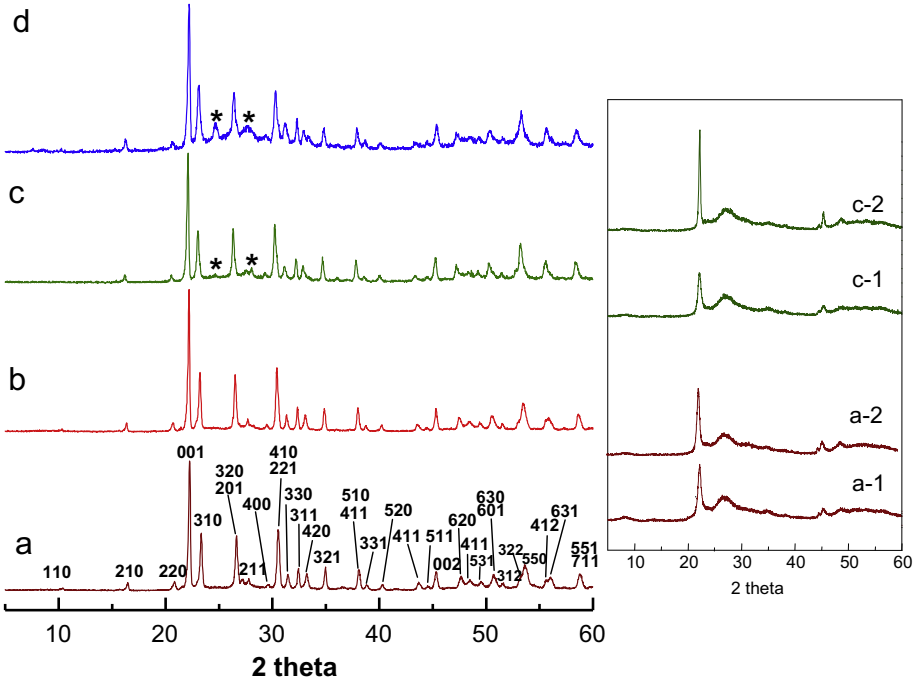

Fig. 2. XRD patterns of catalysts heated at 700 °C: (a) C0-T7; (b) C2-T7; (c) C8-T7; (d) C17-T7. Miller index on pattern has been assigned on the basis of the basic TTB structure. The $Mo_{4.65}V_{0.35}O_{14}$ impurity phase has been marked with an asterisk on patterns c and d. XRD patterns of samples heated at 500 (C0-T5 and C8-T5) and 600 °C (C0-T6 and C8-T6) have also been included for comparison (a1) C0-T5; (a2) C0-T6; (c1) C8-T5; (c2) C8-T6.

heated at lower temperatures (Fig. 2, patterns a_1, a_2, c_1 and c_2). The impurity phase $Mo_{4.65}V_{0.35}O_{14}$ is formed in a certain extension for increasing tellurium concentration and it has been marked in the corresponding patterns when observed (diagrams c and d).

In order to correlate chemical composition and crystal structure, the microstructure of materials heat treated at 700 °C was further analyzed by transmission electron microscopy. The chemical composition of the crystalline phases was determined in the transmission electron microscope by means of crystal by crystal XEDS microanalysis.

Fig. 3 corresponds to the low magnification high-resolution micrograph of a crystal of the C4-T7 catalyst. As observed for this catalyst but in the same way for the whole series, crystals appear to be constituted by big crystalline areas intergrown with amorphous regions. While the amorphous regions can be hardly found in crystals with low tellurium content (C1-T7 and C2-T7), they are easily observed for growing tellurium concentration in the sample (C4-T7 to C17-T7). From the microanalysis performed, it is shown that crystalline areas always give a very similar atomic ratio, independently of the nominal composition of the catalyst (see Table 1). Amorphous regions are mainly constituted by tellurium and molybdenum, and the amount of these amorphous areas clearly increases when the nominal tellurium content of the catalyst increases. Typical XEDS spectra of both areas have been included in Fig. 3.

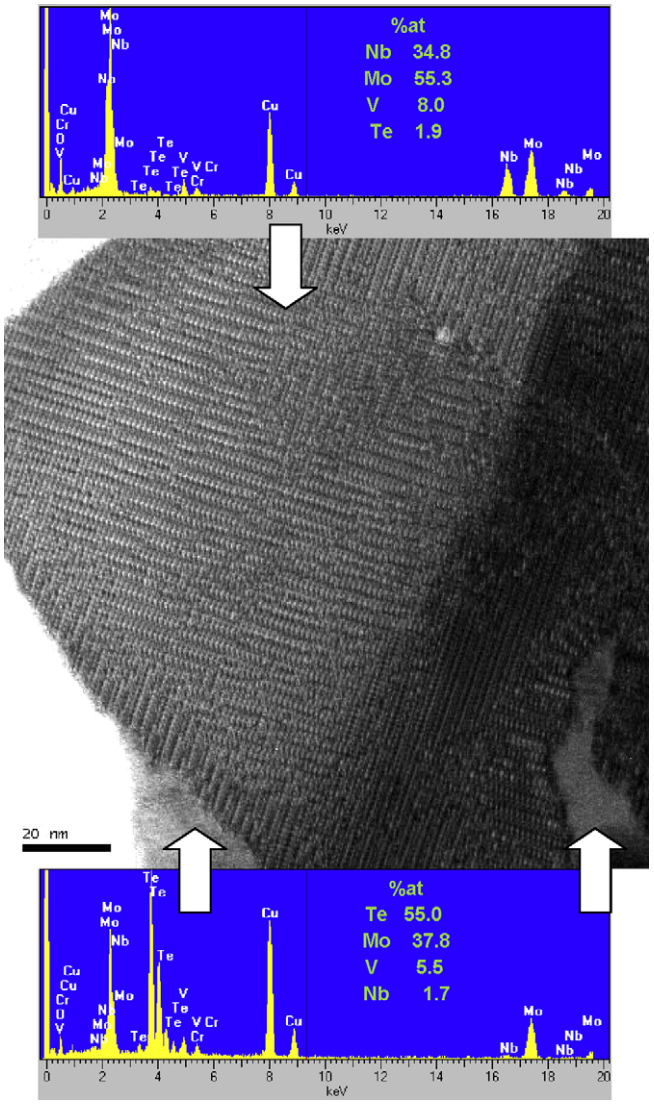

Fig. 3. High-resolution micrograph of an island growth type crystal oriented along $[001]_{TTB}$. Amorphous and crystalline areas are shown together with their corresponding XEDS spectra.

Fig. 4a resembles the electron diffraction pattern of a crystal of the catalyst C4-T7. The pattern corresponds to the [001] projection of the TTB structure, but in addition to the main reflections of the TTB-type substructure diffuse scattering appears centred around them, which might be indicative of short-range order. Its shape is almost circular with radii $r^* \approx 0.33a^*_{TTB}$ and it is specially streaking along $[110]^*_{TTB}$ and $[-110]^*_{TTB}$ directions. The corresponding HREM image is shown in Fig. 4b. Although regular contrast related to the TTB-type framework can be observed in the whole area, which is responsible for the 1.2 nm measured periodicity along $[100]_{TTB}$ and $[010]_{TTB}$, additional irregular contrast can be appreciated at a first glance.

As mentioned in the introduction, short-range ordered structures are formed in the Nb_2O_5/WO_3 system depending on the distribution of filled PC elements. Application of theoretical models is well established and has satisfactorily explained the order–disorder situations of atom strings in ternary Nb–W oxides [21–23]. In these systems, the crystals give diffraction patterns exhibiting well-defined curves of diffuse intensity passing through the positions of the diffraction spots due to the long-range order state. As an example, the electron diffraction patterns of $Nb_7W_{10}O_{47.5}$ (O/M = 2.79) present diffuse scattering located on circles of two different radii: $r \approx 0.33a^*_{TTB}$ and $r \approx 0.4a^*_{TTB}$ [24]. The former is related to the threefold TTB superstructure of the composition Nb_2O_5:WO_3:4:9 ($Nb_8W_9O_{47}$), and the latter, previously observed for the compositions Nb_2O_5:WO_3 of 3:8 and 17:48 [21–23], is associated with the ordered structure of $Nb_6W_8O_{39}$.

$Nb_8W_9O_{47}$-type structure represents a very stable phase in the Nb_2O_5-WO_3 system, whose formation is also favoured for other compositions by keeping the oxygen/metal ratio 47:17 (O/M = 2.76). The solid solution series $Nb_{8-n}W_{9+n}O_{47}$ ($1 \leqslant n \leqslant 5$) has been prepared by the substitution of $2Nb^{5+}$ by Nb^{4+} (or W^{4+}) and W^{6+} leading to oxides $M_{17}O_{47}$ (M = Mo, W) with mixed valence and varying the Nb:W ratio [27]. The threefold superstructure of TTB is maintained, which is the pentagonal bipyramidal site preferentially occupied by niobium [28].

Providing our experimental observations, a clear correspondence between the structural features observed in the reciprocal lattice of the samples under study and those of the Nb_2O_5/WO_3 system can be established. In this sense and according to the corresponding electron diffraction pattern on Fig. 4a, contrast in the image of Fig. 4b can be interpreted as coming from a disordered distribution of filled PC in a well-ordered basic TTB framework which is now constituted by niobium, molybdenum and vanadium. Order at the short-range can also be clearly appreciated when observing the image contrast in Fig. 3. In spite of the low magnification and the crystal thickness, small fringes of 10 to 20 nm with the periodicity of the threefold superstructure of $M_{17}O_{47}$ can be measured in the two perpendicular directions, showing a lack of long-range order.

The fact that in our materials only short-range ordered structures derived from the TTB-type cell are observed indicates that the ratio of the atomic components is not adequate to obtain the threefold superstructure of the 4:9 phase. The atomic distribution in the ordered 4:9 phase leads to a $Nb_{PC}/(Mo + Nb)_{skeleton}$ (in which Nb_{PC} is the number of Nb atoms in PC) ratio of 0.133. The total atomic Nb/Mo ratio is 0.88. As previously mentioned, TTB-type crystalline areas of the crystals of our catalysts series present a roughly constant atomic composition (~57% Mo, ~30% to 33% Nb, ~6% to 8% V and 1.5% to 3%) for all the investigated samples (see Table 1). It is important to note that although nominal tellurium content markedly varies from one sample to the other, it

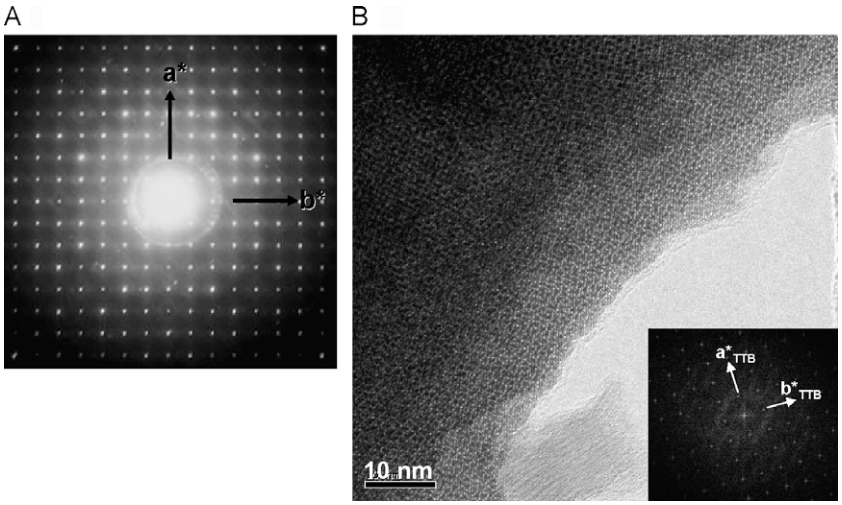

Fig. 4. (a) Selected Area Electron Diffraction (SAED) pattern corresponding to a crystal of the catalyst C4-T7. Reciprocal directions refer to the basic TTB unit cell ([001] projection). (b) High-resolution electron micrograph of a crystal of the C4-T7 catalyst projected on the $[001]_{TTB}$ zone axis, showing the irregular contrast coming from the disordered distribution of filled pentagonal tunnels. The corresponding Fourier transform has been included.

seems to enter in the structure in a regular atomic percentage. The fact that XEDS microanalysis shows a constant Te content in the crystalline areas, whatever the nominal Te content is, can be taken as a demonstration of the incorporation of tellurium into the TTB framework. Otherwise, distribution of tellurium on the surface of the crystals should be observed, when occurred, in the TEM images either if it is in the form of TeO_2 or as an amorphous phase. Another experimental evidence that may support that tellurium is in the bulk of the structure is the fact that when crystals are thin enough crystal surface begins to show the formation of small balls of sublimated tellurium atoms. This fact probes by one side that tellurium, when present on the crystal surface, can be viewed by TEM and by other side that tellurium evolves from the bulk of the crystals. Although these results provide evidence that Te is part of the structure, the total incorporation of Te in the framework of the TTB structure is still not absolutely confirmed.

We can assume that molybdenum and vanadium atoms are preferentially placed in the MO_6 octahedra because of their smaller cationic size. Niobium must contribute to the skeleton formation as well, a certain amount being distributed in the pentagonal columns. From the above-mentioned considerations, and taking into account that Nb/(Mo + V) ratio is 0.49, it can be noticed that there is some niobium deficiency that probably hinders the long-range ordered distribution of filled pentagonal columns. In addition, tellurium must compete with the niobium atoms in the occupancy of the tunnels.

Moreover, and although crystals of catalyst C0-T7 do not contain the amorphous areas, we have not found structural differences between the crystalline zones of samples containing tellurium and those without tellurium.

Infrared spectra of catalysts heat treated at 700 °C are presented in Fig. 5. The Te-free sample shows broad bands at 885, 752, 630 and 528 cm^{-1}, in addition to a shoulder at 991 cm^{-1} (Fig. 5a). According to the previous results reported for Mo-containing bronzes [25], the low-frequency signal is related to isolated oxomolybdenum species, i.e. terminal Mo = O stretching vibrations, while the high-frequency bands are related to Mo–O–Y (Y = Mo, V, Nb) bridge vibrations. The appearance of broad bands can be related to an important heterogeneity in the Mo–O–Y bridges in Mo-based bronzes [29–31].

The same features can be observed in the spectra corresponding to Te-containing samples (Fig. 5, spectra b–e), therefore indicating that the average crystalline structure is not modified by the incorporation of tellurium atoms. However, since the IR spectra of amorphous and crystalline TeO_2 show bands at 665 or 665 and

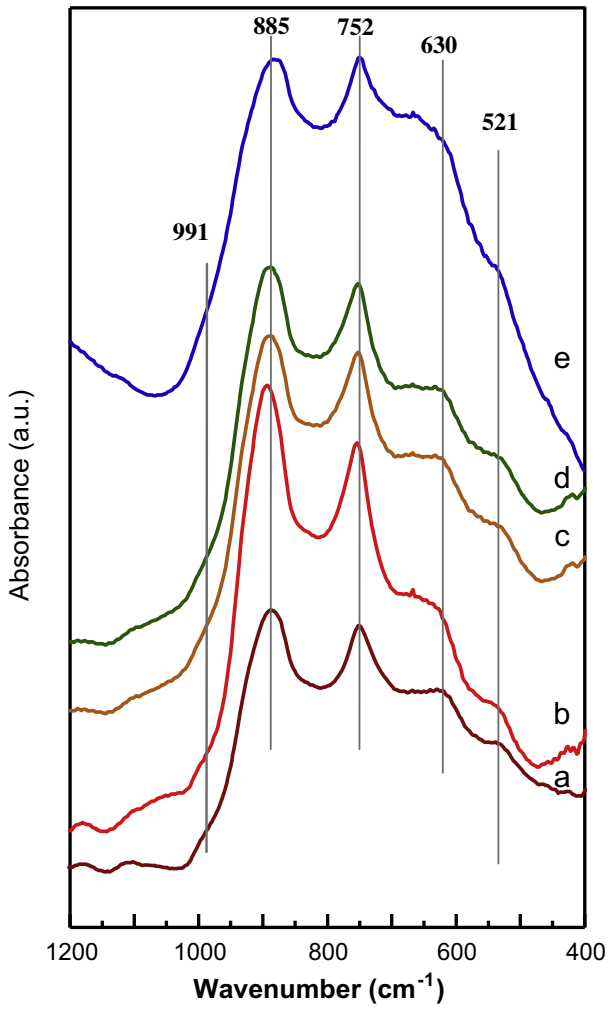

Fig. 5. FTIR spectra of catalysts: (a) C0-T7; (b) C2-T7; (c) C4-T7; (d) C8-T7 and (e) C17-T7.

774 cm^{-1} [31,32], respectively, the absence of TeO_2 cannot be completely ruled out.

Fig. 6 shows the IR spectra of Te-free (Fig. 6, spectra a to c) and Te-containing samples (Fig. 6, spectra d to f) heat treated at 500, 600 and 700 °C. Although the same bands are apparently observed in all cases, the width of the band at 881 cm^{-1} decreases (maybe by the disappearance of a second band at ca. 920 cm^{-1}) when the heating temperature increases. Since the high-frequency bands can be related to Mo=O double bond stretching vibrations [29–31], it can be proposed that pseudoamorphous samples present slightly different Mo-sites than those observed in well-crystallized catalysts. However, the Mo–O–Y vibrations seem to be very similar in both pseudoamorphous and TTB-type phases. Moreover, the band at 1113 cm^{-1} in Fig. 6 is related to P–O–P stretching modes of the PO_4 tetrahedra [33].

Fig. 7 shows the DR UV–vis spectra of catalysts. Two different regions at 200 to 450 and 500 to 700 nm can be analyzed. The spectra show a great similarity to those previously reported for MoTeVNbO catalysts constituted by the orthorhombic M1 and the pseudohexagonal M2 phases, respectively [26], as well as for other Mo-containing bronzes [29–31]. Bands observed in the 500 to 750 nm range are related to the presence of Mo and V in oxidation states lower than 6+ and 5+, respectively, but the assignment of bands in the 200 to 450 nm range is a difficult task because the signals of many species converge, i.e. Mo(VI) (250 to 400 nm) [31,34,35], V(V) (250 to 450 nm) [33,36], Te(IV) (250 to 300 nm) [26] and Nb(V) (235 to 310 nm) [37]. On the other hand, the maximum about 550 to 600 nm corresponds to the presence of Mo^{5+} [31,35,38], although the exact position strongly depends on the Mo(VI)/Mo(V) ratio. This band can overlap with bands in the range 620 to 750 nm due to the presence of V^{4+} [36]. In spite of the difficulties of a precise assignment, we can conclude that Mo^{6+}, V^{4+}, Te^{4+} and Nb^{5+} are mainly present in our catalysts. The intensity ratio between the broad band observed in the 500 to 800 nm range and the band observed in the 200 to 450 nm range in Te-free sample (Fig. 7, spectrum a) is lower than that observed in Te-containing catalysts (Fig. 7, spectra b-d), suggesting a higher average oxidation state for Mo and V species in the Te-free catalyst.

The bulk and surface elemental compositions are presented in Table 1. For comparison, the variation of the Te/Mo atomic ratio in the bulk and surface is shown in Fig. 8. A surface Te enrichment is observed for samples with high Te loading suggesting a partial deposition of Te on the catalyst surface. This could be due to the formation of an amorphous Te-enriched phase when the amount

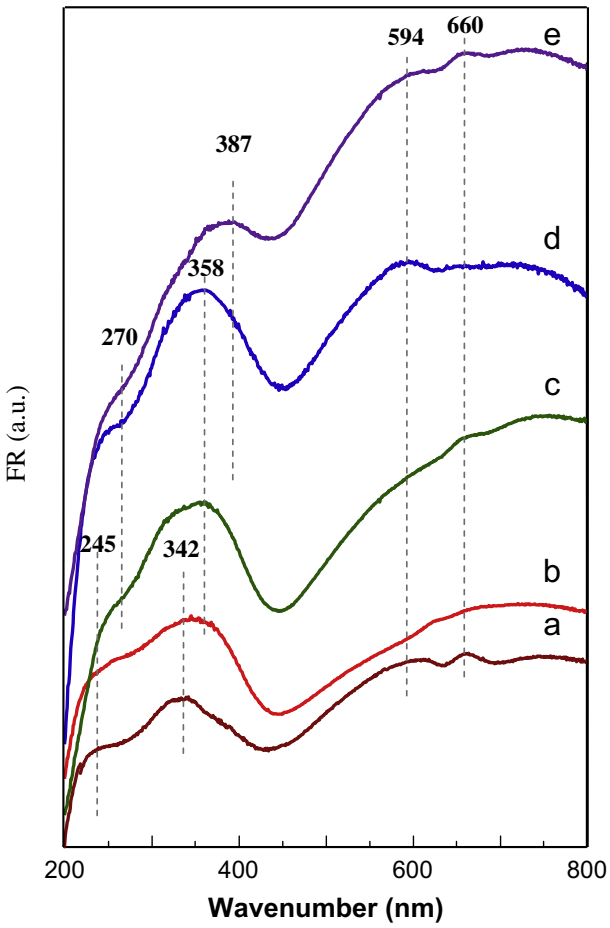

Fig. 7. DR UV–vis spectra of catalysts: (a) C0-T7; (b) C2-T7; (c) C4-T7; (d) C8-T and (e) C17-T7.

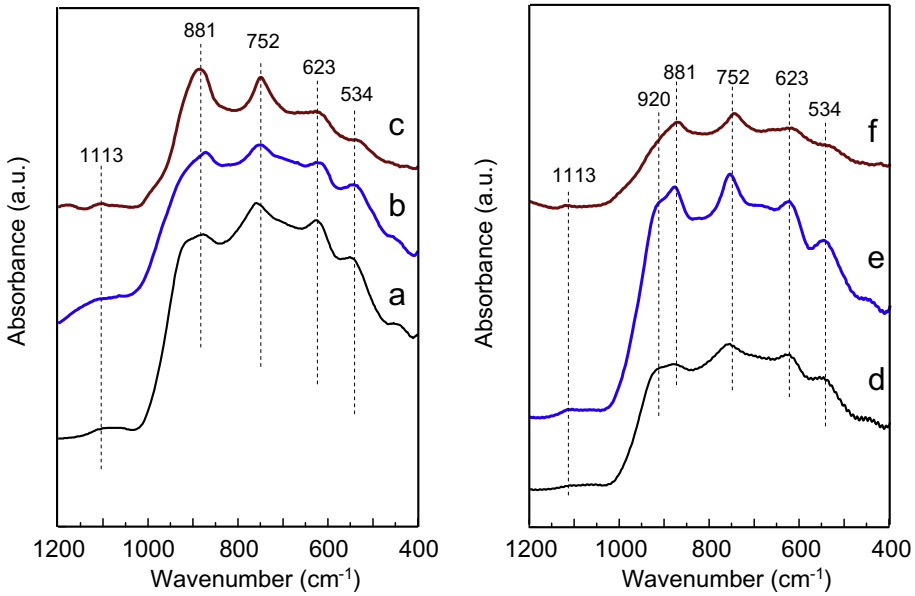

Fig. 6. FTIR spectra of catalysts: (a) C0-T5; (b) C0-T6; (c) C0-T7; (d) C8-T5; (e) C8-T6 and (f) C8-T7.

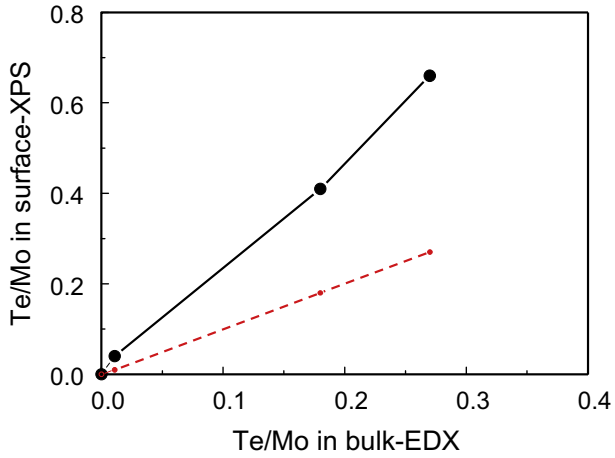

Fig. 8. Surface vs bulk Te/Mo ratio as determined, respectively, by XPS and EDX analyses (solid line). See the deviation from theoretical coincident Te/Mo ratios in surface and bulk (dashed line).

of Te exceeds the Te/Mo ratio needed to incorporate Te in the TTB structure.

The XPS results of some catalysts are shown in Table 2. Well-resolved Mo $3d_{5/2}$, Nb $3d_{5/2}$, V $2p_{3/2}$, P $2p$ and Te $3d_{5/2}$ XPS bands whose intensities depend on the chemical composition have been observed (Fig. 9). The Mo $3d$ core-level spectra of catalysts show that the binding energy of the Mo $3d_{5/2}$ is similar for all the samples (232.6 to 232.9 eV). The observed differences in the binding energies are not significant and are slightly higher than that of pristine MoO_3 (232.5 eV). Since the binding energy of MoO_3 is 232.5 eV, while Mo^{5+} cations are observed at 232.0 eV [39], the results of Table 2 suggest the main presence of Mo^{6+} on the catalyst surface. In the same way, the Nb $3d$ and V $2p$ core-level spectra of the catalysts are similar, presenting Nb $3d_{5/2}$ and V $2p_{3/2}$ binding energies at ca. 206.9 to 207.2 eV and 516.7 to 516.9 eV, respectively (Table 2), and suggesting the main presence of Nb^{5+} [40] and V^{5+} [41,42] ions at the surface. No significant variations of their corresponding peak widths were observed in both Te-free and Te-containing samples.

The Te $3d$ core-level spectra of the catalysts indicate that the binding energy of the Te $3d_{5/2}$ changes from 576.9 to 576.4 eV. Since the B.E. corresponding to Te^{4+} is 576.2 eV, in H_6TeO_6 it is observed at 577.3 eV [43,44], we must conclude the presence of Te^{4+}ions on the surface of these catalysts. On the other hand, the binding energy of the P $2p$ photoemission corresponds to the presence of P^{5+} [43], and decreases with the incorporation of Te^{4+} from 134.0 to 133.5 eV (Table 2).

3.2. Propene oxidation on Te-containing catalysts

Table 3 shows the catalytic data for the oxidation of propene. For comparison, the catalytic results obtained over MoVTeNbO mixed metal oxides, constituted by pure M2 phase, have also been included. Acrolein, acrylic acid (at high olefin conversions), carbon monoxide and carbon dioxide have been the main reaction products on TTB-based catalysts, although acetic acid, acetone and acetaldehyde have also been obtained as minor products. In addition, the Te-free catalyst yields only traces of acrolein, whereas Te-containing samples can reach selectivity to acrolein higher than 90% (Table 4).

Fig. 10 plots the variation with the tellurium content of (i) the propene conversion and (ii) the selectivity to partial oxidation products (acrolein + acrylic acid at isoconversion conditions, i.e. 40%) obtained during the propene oxidation at 380 °C over the TTB-based catalysts. It can be seen that both the propene conversion and the areal rate of propene oxidation decrease when the Te/Mo atomic ratio in catalysts increases with Te/Mo ratios higher than 0.02 (Table 3). In an opposite trend, the selectivity to partial oxidation products, i.e. acrolein and acrylic acid, initially increases with the Te content until a Te/Mo ratio in bulk of 0.03. For higher Te contents no appreciable changes in the selectivity to partial oxidation products are observed.

Fig. 11 shows the variation of the yield to partial oxidation products (acrolein and acrylic acid) with the Te content of catalysts. The value initially increases and a maximum is reached at a bulk Te/Mo atomic ratio of 0.03. At higher Te loadings, the yield to acrolein drops due to the decrease in the propylene conversion. We must indicate that a rate of formation of acrolein per unit of mass and unit of time (STY) of ca. 40 $g_{acrol}\,h^{-1}\,kg_{cat}^{-1}$ has been achieved at 380 °C over sample C3-T7, which is higher to that achieved over the catalyst presenting M2-phase, i.e. CAT-2 (Table 1).

It has been observed that the incorporation of tellurium in molybdate-based catalysts has a strong influence on their catalytic performance in olefin partial oxidation [45,46]. This has been explained by both the creation of allylic abstraction sites (mainly related to the presence of Te sites) and the modification of Mo=O double bonds [12,14,25,45–50]. A similar explanation can be proposed in the case of TTB-based catalysts with Te/Mo ratios in bulk lower than 0.03.

However, other aspects must be considered in the case of catalysts with higher Te/Mo contents. At this point, the complexity inherent to the multicomponent system, i.e. Mo–Nb–V–P–Te–O, makes extremely difficult to carry out a rationalization of the catalytic behaviour, as already done in binary oxides [51]. In this way, synergism due to a cooperation between phases should also be considered [51–55].

Nevertheless, and according to the structural characterization (HREM), it can be said that the lower propene conversion and the yield of acrolein observed over catalysts with higher Te content are explained by the increasing presence of the amorphous Te-enriched phase (which is also related to the Te enrichment of the catalyst surface as suggested from the XPS results). At this point, we must indicate that Te–Mo mixed oxides are active and selective in the oxidation of propylene to acrolein in excess of Mo [56], while Te-rich Te–Mo–O mixed oxides present a very low catalytic activity in propylene oxidation [57]. For this reason, since Te-rich catalysts present a lower amount of active phase per weight of catalyst, the amorphous areas observed by TEM in our catalysts should have

Table 2
Binding energy of Mo, Nb, V, P, Te and O XPS for TTB catalysts.

Catalyst	Mo $3d_{5/2}$ (eV)	Nb $3d_{5/2}$ (eV)	V $2p_{3/2}$ (eV)[a]	P $2p$ (eV)	Te $3d_{5/2}$ (eV)	O $1s$ (eV)
C0-T7	232.9	207.2	516.9 (1.88)	134.0	–	530.6
C1-T7	232.6	206.9	516.9 (2.01)	133.4	576.4	530.4
C4-T7	232.7	206.9	516.8 (1.88)	133.5	576.5	530.4
C8-T7	232.9	207.2	516.7 (2.00)	133.5	576.8	530.8

[a] The FWHM for V $2p_{3/2}$ peak is given in parenthesis.

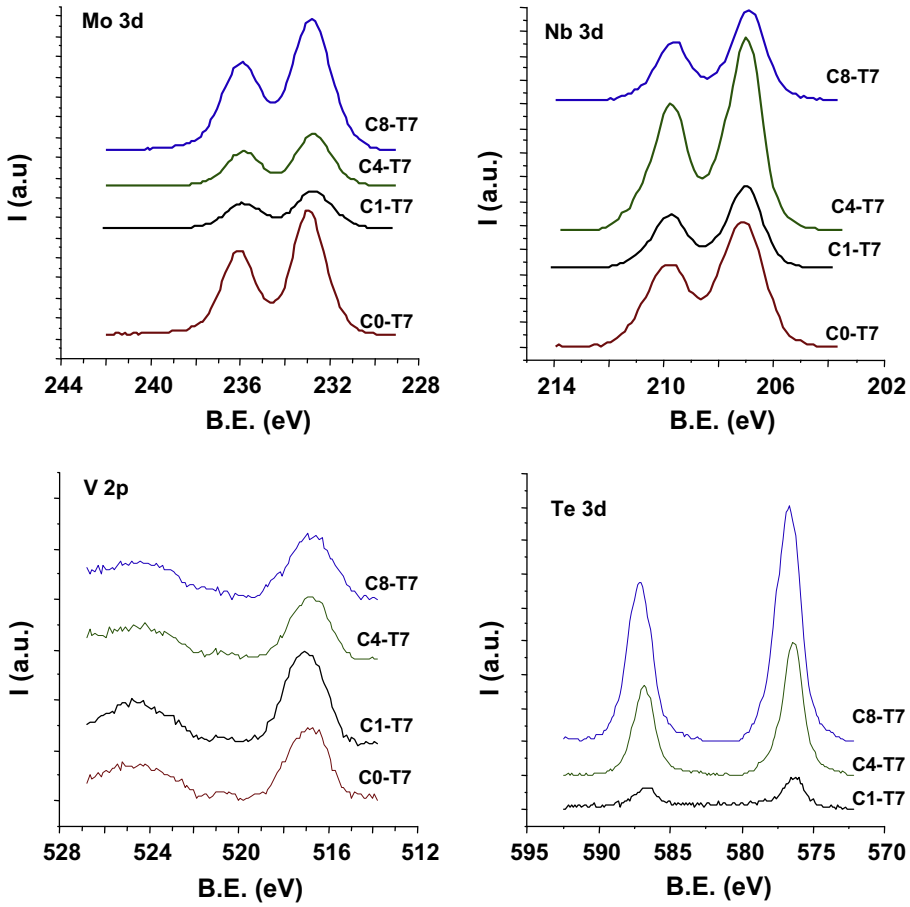

Fig. 9. Photoelectron spectra corresponding to the main transitions (Mo 3*d*, Nb 3*d*, V 2*p*, P 2*p* and Te 3*d*) of TTB catalysts: (a) C0-T7; (b) C1-T7; (c) C4-T7 and (d) C8-T7.

Table 3
Selective oxidation of propylene over Mo-based catalysts.[a]

Catalyst	Te/Mo in bulk[b]	Conversion (%)	Selectivity (%)							STY[c]	Areal rated[d]
			Acrolein	Acrylic acid	Acetaldehyde	Acetone	AcOH	CO	CO_2		
C0-T7	0	57.8	2.2	0.9	1.3	1.5	19.4	56.4	18.2	1.9	8.9
C1-T7	0.01	55.1	6.1	1.0	0.8	1.4	13.2	56.7	20.8	4.0	8.8
C2-T7	0.02	58.7	52.3	1.1	2.2	2.0	1.1	28.7	12.5	32.3	9.0
C3-T7	0.03	43.7	89.0	3.2	1.0	0.2	0.9	3.8	1.8	39.7	6.9
C4-T7	0.15	22.3	91.7	1.6	1.0	2.8	t	1.5	1.4	21.5	3.5
C8-T7	0.23	17.8	91.2	t	1.4	3.5	t	2.3	1.6	16.7	2.9
C17-T7	0.40	14.0	92.3	t	0.9	1.9	t	1.5	3.5	13.3	2.3
CAT-M2[f]	0.58	9.7	8.6	69.5	0.3	6.5	1.9	6.5	6.0	10.1[e]	–

[a] Reaction conditions: 380 °C, $C_3^=/O_2/He/H_2O$ molar ratio of 1.5/6/77.5/15 and contact time, W/F, of 543 g_{cat} h $(mol_{C3})^{-1}$.
[b] Bulk Te/Mo atomic ratio in catalyst.
[c] Rate of formation of acrolein at 380 °C per unit mass of catalyst, STY, in g_{acrol} h^{-1} kg_{cat}^{-1}
[d] Catalytic activity of propane oxidation normalized per surface area, in 10^3 $g_{C_3H_6}$ h^{-1} m^{-2}.
[e] Rate of formation of acrylic acid at 380 °C per unit mass of catalyst, STY, in g_{AA} h^{-1} kg_{cat}^{-1}
[f] MoVTeNb mixed oxide catalyst with M2 phase prepared as in Ref. [25].

Table 4
Influence of the heating temperature of catalysts on their catalytic performance in partial propylene oxidation.

Catalyst	Heating temperature (°C)	Crystalline phase (XRD)[a]	W/F (in g_{cat} h $(mol_{C3})^{-1}$)[b]	Conv. (%)[c]	Selectivity (%)				
					Acrolein	Acrylic acid	CO	CO_2	Others[d]
C8-T7	700	TTB phase	1876	43.5	81.5	11.6	2.7	1.7	2.4
C8-T6	600	Pseudoamorphous	136	37.1	1.6	84.5	7.7	4.3	1.9
C8-T5	500	Pseudoamorphous	72	40.2	1.0	81.8	8.6	6.1	2.4

[a] A pseudoamorphous material, presenting a XRD peak at $2\theta = 22.0°$, is observed in samples heat treated at 500 or 600 °C.
[b] Different contact times, W/F in g_{cat} h $(mol_{C3})^{-1}$, have been used to give a propene conversion of ca. 40%.
[c] Reaction conditions: 380 °C, $C_3^=/O_2/He/H_2O$ molar ratio of 1.5/6/77.5/15.
[d] Acetic acid and acetone.

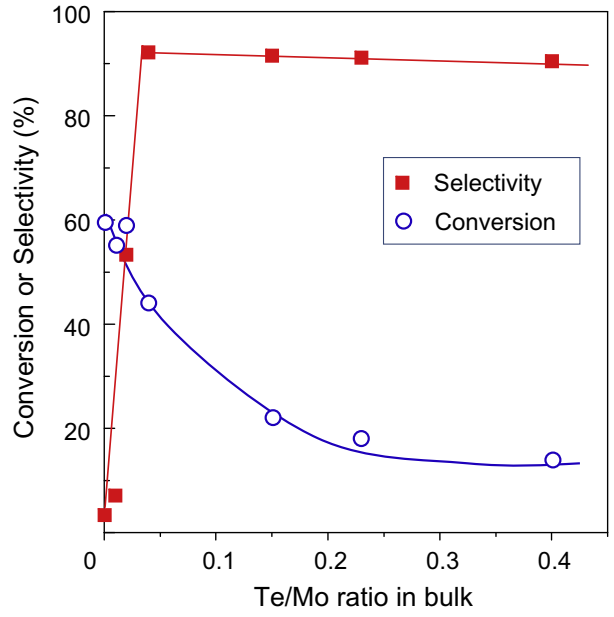

Fig. 10. Influence of the Te/Mo atomic ratio of the catalysts on the propylene conversion (a) and on the selectivity to acrolein + acrylic acid (b). Reaction temperature 380 °C; W/F = 540 g_{cat} h $(mol_{C3})^{-1}$.

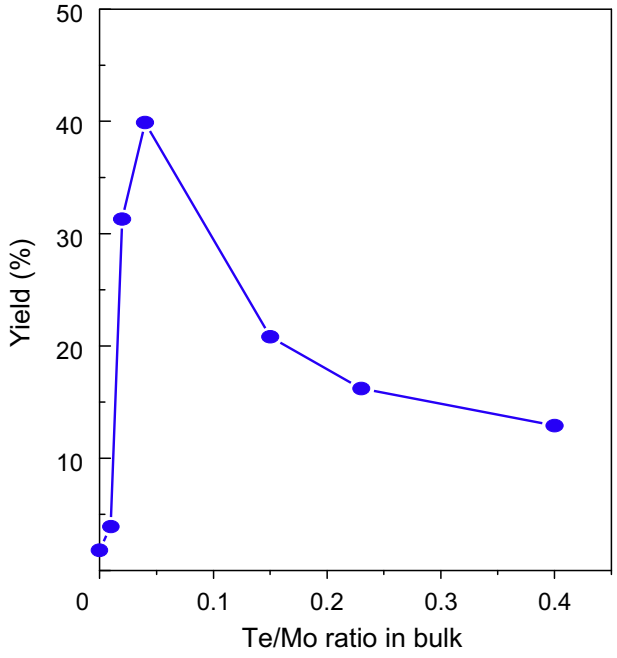

Fig. 11. Influence of the Te/Mo atomic ratio of the catalysts on the yield to partial oxidation products (acrolein and acrylic acid) obtained during the propylene oxidation at 380 °C on TTB-based catalysts. Reaction conditions as in Fig. 10.

a negative influence in the catalytic activity of catalysts with high Te/Mo ratios.

Fig. 12 shows the evolution of the selectivity to the main reaction products (acrolein, acrylic acid, CO and CO_2) with the propylene conversion for some selected catalysts. It can be observed that the formation of acrylic acid begins to be important at olefin conversions over 40%. This behaviour is different from that observed over catalyst CAT-M2 in which a high selectivity to acrylic acid is also observed at low propene conversion. Thus, acrolein is favoured in TTB-based catalysts, while acrylic acid is more favoured over HTB-like structures as in CAT-M2 sample suggesting a strong influence of the crystalline structure on both the nature and the selectivity of partial oxidation products.

The above-mentioned results are in agreement with those achieved on other Mo-based bronzes with orthorhombic (OTB) [9–14] or hexagonal (HTB) structures [25] in which Te plays a key role in the activation of olefins. Accordingly, the synthesis of new Mo-containing bronzes can be a way to improve the catalytic performance in alkane and olefin partial oxidation. The catalyst structure seems to be a key factor in both hydrocarbon activation and the nature of reaction products. Thus, OTB structure (with heptagonal, hexagonal and pentagonal channels) is active in alkane oxidation [9–12,14], while HTB (with hexagonal channels) [14,25] and TTB (with pentagonal channels) are only active in olefin oxidation.

On the other hand, the chemical composition of the catalysts seems to be also of high influence on catalytic behaviour, although the particular role of each element is not clear. MoVTeNbO catalysts with HTB structure are very selective in the oxidation of propene to acrylic acid, while MoVTeO catalysts are only selective in the oxidation of propene to acrolein [39].

In a first approach, one could conclude the importance of Nb^{5+} sites in the formation of acrylic acid. However, although the importance of the presence of Nb in the selectivity to acrylic acid has been proposed on catalysts with OTB structure [47,48,52], Nb-free catalysts also present a relative high selectivity to acrylic acid during the oxidation of propane or propene [49,50]. Therefore, other aspects should be considered in order to explain the high selectivity to acrolein (and the low formation of acrylic acid) in the case of Nb-containing catalysts with a TTB structure.

3.3. The importance of the crystalline phase in catalytic performance

As it had been previously detailed, the formation of TTB-type materials requires a heating temperature of 700 °C, whereas pseudoamorphous materials are obtained at lower temperatures. Table 4 shows the influence of the calcination temperature on the catalytic behaviour for propene oxidation as well as the distribution of the reaction products obtained over a representative Te-containing catalyst, i.e. C8-T7. In this case, the contact time, W/F, was varied in order to achieve similar propene conversions. It can be seen that pseudoamorphous materials are more active than the sample heat treated at 700 °C. Thus, C8-T7 catalyst is 10 to 15 times less reactive than that heated at 600 °C.

This behaviour is quite different from that observed over MoVTeNbO bronze catalysts with orthorhombic structure (OTB), in which amorphous materials present a catalytic activity similar or lower than those presenting OTB structure [5].

On the other hand, the partial oxidation products formed during propene oxidation over these catalysts strongly depend on the heating temperature. Thus, at the same propene conversion, pseudoamorphous materials are very selective to acrylic acid, while catalysts with TTB structure are very selective to acrolein. It is noteworthy that selectivity towards the two partial oxidation products, i.e. acrolein and acrylic acid, is slightly higher using the TTB-type material than using the pseudoamorphous catalysts. These results seem to indicate that the crystalline structure has a strong influence on catalytic behaviour as it had been previously suggested in the case of MoVTeNbO catalysts. It means that the transformation of pseudoamorphous materials to the TTB-type structure during the heating process step favours a blockage of (i) the active sites for the partial oxidation of acrolein to acrylic acid and (ii) some unselective sites to yield carbon oxides. However, alternatively, pseudoamorphous materials (which are not detected in the case of catalyst heated at 700 °C) could play some role in the formation of acrylic acid, as it has been recently suggested

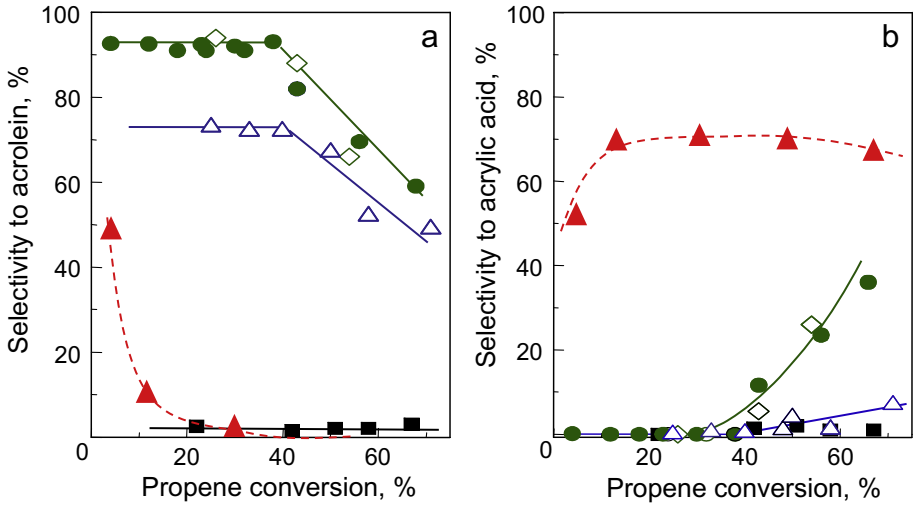

Fig. 12. Variation of the selectivity to acrolein (a) and acrylic acid (b) with the propene conversion obtained at 380 °C over TTB catalysts with different Te/Mo ratios. Catalyst: C0-T7 (■); C2-T7 (Λ); C3-T7 (◊); C8-T7 (●). For comparison, the catalytic results achieved over CAT-M2 (▲) are also presented.

when working with catalysts with an orthorhombic structure [58]. We must indicate that active and selective catalysts for the selective oxidation of acrolein to acrylic acid are based in MoVW mixed oxides with amorphous and $(MoVW)_5O_{14}$-type crystals [59,60]. However, in an opposite trend, the presence of other elements, such as tellurium, in amorphous materials (as occurs in Nb-free M2-crystals [13]) can eliminate the consecutive oxidation of acrolein to acrylic acid. In this sense, it has been recently reported that although crystalline M2 catalysts yield acrylic acid, their formation of acrylic acid is drastically reduced if the M2 crystals are overlaid with Te–molybdates [61].

On the other hand, and although no apparent structural role has been found for tellurium atoms, the catalysts characterization performed shows the importance of its presence in a certain concentration.

4. Conclusions

In conclusion, Te-containing multicomponent catalysts presenting a tetragonal tungsten bronze (TTB) structure can be achieved from solid prepared hydrothermally from an aqueous solution of molybdophosphoric acid, vanadyl sulphate, niobium oxalate and telluric acid and are finally heated to 700 °C in N_2. However, pseudocrystalline materials are formed when the solid prepared hydrothermally is heated to 500 to 600 °C.

The characterization results of the catalysts indicate that the presence of tellurium does not play a particular structural role in the formation of TTB structure. However, the importance of its presence in a certain concentration is evident . Thus, it has been observed that this type of crystals appears in the form of crystalline islands grown together with an amorphous matrix. The amorphous regions increase when the Te content in the catalysts increases.

The catalytic performance of these catalysts strongly depends on the Te content. The catalytic activity does not vary at Te/Mo ratios in bulk lower than 0.03 but on catalysts with higher Te/Mo contents it decreases when the Te content increases. In a different way, the selectivity to acrolein increases up to a maximun of ca. 90% when the Te/Mo ratio increases in bulk up to ca. 0.03, but it then remains constant for catalysts with higher Te contents. This behaviour can be explained by the nature of Te species in the catalysts. Te atoms seem to be initially incorporated in the framework of the TTB structure up to a Te/Mo ratio in bulk close to 0.03, with the remaining being allocated in a Te-rich amorphous matrix. In this sense, the decrease in the catalytic activity in samples with high Te/Mo ratio is explained by the presence of more or less amorphous matrix in the catalyst, considering the poor activity of Te-rich mixed oxides. Since the higher propylene conversion is observed in catalysts without Te, Mo-containing amorphous phase, it can be concluded that TTB structure is active in the oxidation of propene. However, the higher selectivity to acrolein is explained by the modification of the active sites with the incorporation of Te atoms in framework positions as it was also observed in Te-doped metal molybdates.

On the other hand, high selectivity to acrolein is observed on catalysts with TTB structure (samples heat treated at 700 °C), while high selectivity to acrylic acid is observed for catalysts heat treated at 500 to 600 °C. However, we must indicate that this behaviour is also observed in other bronze-type catalysts. Thus, it had been previously reported that propene is selectively transformed into acrolein (Nb-free MoVTe mixed oxide with M2 phase) or acrylic acid (over Mo–Te–V–Nb containing bronzes with orthorhombic or hexagonal structures). Thus, the different behaviours observed over catalysts depending on the heating temperature can be related to the catalyst structure. However, the appearance of Te, Mo-matrix in catalysts with high Te content could hinder the consecutive oxidation of acrolein to acrylic acid.

Acknowledgments

Financial support from DGICYT in Spain through Projects CTQ2006-09358/BQU, MAT-2006-09358 and MAT2007-61954 is gratefully acknowledged. Authors are also grateful to the Centro de Microscopía Electrónica (U.C.M.) for facilities.

References

[1] M. Hatano, A. Kayo, EP 318285B1, 1988.
[2] T. Ushikubo, K. Oshima, A. Kayo, T. Umezawa, K. Kiyono, I. Sawaki, EP529853 A2, Mitsubishi Chemical Industries, 1993.
[3] T. Ushikubo, K. Oshima, A. Kayou, M. Hatano, Stud. Surf. Sci. Catal. 112 (1997) 473.
[4] J.M. López Nieto, P. Botella, M.I. Vázquez, A. Dejoz, WO0346035, 2003.
[5] P. Botella, E. García-González, A. Dejoz, J.M. López Nieto, M.I. Vázquez, J.M. González-Calbet, J. Catal. 225 (2004) 428.
[6] W. Ueda, N.F. Chen, K. Oshihara, Chem. Commun. (1999) 517.
[7] D. Vitry, Y. Morikawa, J.L. Dubois, W. Ueda, Appl. Catal. A: Gen. 251 (2003) 411.
[8] H. Watanabe, Y. Koyasu, Appl. Catal. A: Gen. 194–195 (2000) 479.

[9] P. Botella, J.M. López Nieto, A. Martinez-Arias, B. Solsona, Catal. Lett. 74 (2001) 149.
[10] J.M.M. Millet, H. Roussel, A. Pigamo, J.L. Dubois, J.C. Jumas, Appl. Catal. A: Gen. 232 (2002) 77.
[11] H. Tsuji, K. Oshima, Y. Koyasu, Chem. Mater. 15 (2003) 2112.
[12] (a) P. DeSanto, D.J. Buttrey, R.K. Grasselli, C.G. Lugmair, A.F. Volpe, B.H. Toby, T. Vogt, Z. Krist. 219 (2004) 152;
(b) P. DeSanto, D.J. Buttrey, R.K. Grasselli, C.G. Lugmair, A.F. Volpe, B.H. Toby, Top. Catal. 23 (2003) 23.
[13] E. García-González, J.M. López Nieto, P. Botella, J.M. González-Calbet, Chem. Mater. 14 (2002) 4416.
[14] P. Botella, E. García-González, J.M. López Nieto, J.M. González-Calbet, Solid State Sci. 7 (2005) 507.
[15] P. Botella, B. Solsona, E. García-González, J.M. González-Calbet, J.M. López Nieto, Chem. Commun. (2007) 5040.
[16] P. Botella, B. Solsona, J.M. López Nieto, Catal. Today 141 (2009) 311.
[17] M. Lundberg, M. Sundberg, A. Mágneli, J. Solid State Chem. 44 (1982) 32.
[18] B.-O. Marinder, Angew. Chem., Int. Ed. 25 (1986) 431.
[19] M.W. Viccary, R.J.D. Tilley, J. Solid State Chem. 104 (1993) 131.
[20] S. Iijima, J.G. Allpress, Acta Cryst. A 30 (1974) 22.
[21] S. Iijima, J.M. Cowley, J. Phys. Colloq. 38 (1977) 135.
[22] R. De Ridder, G. Van Tendeloo, D. Van Dyck, S. Amelinckx, Phys. Stat. Sol. A 41 (1977) 555.
[23] S. Horiuchi, K. Muramatsu, Y. Matsui, J. Appl. Cryst. 13 (1980) 141.
[24] F. Krumeich, Acta Cryst. B 54 (1998) 240.
[25] P. Botella, J.M. López Nieto, B. Solsona, Catal. Lett. 78 (2002) 383.
[26] J.M. López Nieto, P. Botella, B. Solsona, J.M. Oliver, Catal. Today 81 (2003) 87.
[27] F. Krumeich, A. Hussain, C. Bartsch, R. Gruehn, Z. Anorg. Allg. Chem. 621 (1995) 799.
[28] F. Krumeich, M. Wörle, A. Hussain, J. Solid State Chem. 149 (2000) 428.
[29] P. Afanasiev, J. Phys. Chem. B 109 (2005) 18293.
[30] F. Cariati, J.C.J. Bart, A. Sgamellotti, Inorg. Chim. Acta 48 (1981) 97.
[31] J.C.J. Bart, F. Cariati, A. Sgamelloti, Inorg. Chim. Acta 36 (1979) 105.
[32] H. Zhang, M.T. Swihart, Chem. Mater. 19 (2007) 1290.
[33] Z.-T. Zhu, J.L. Musfeldt, Z.S. Teweldemedhin, M. Gremblatl, Chem. Mater. 13 (2001) 2940.
[34] H. Aritani, T. Tanaka, T. Funabiki, S. Yoshida, K. Eda, N. Sotani, M. Kudo, S. Hasegawa, J. Phys. Chem. 100 (1996) 19495.
[35] V.R. Porter, W.B. White, R. Roy, J. Solid State Chem. 4 (1972) 250.
[36] P. Blasco, P. Concepción, J.M. López Nieto, J. Pérez-Pariente, J. Catal. 152 (1995) 1.
[37] J.M.R. Gallo, I.S. Paulino, U. Schuchardt, Appl. Catal. A: Gen. 266 (2004) 223.
[38] J.C.J. Bart, G. Petrini, N. Giordano, Z. Anorg. Allg. Chem. 413 (1975) 180.
[39] P. Botella, J.M. López Nieto, B. Solsona, A. Mifsud, F. Márquez, J. Catal. 209 (2002) 445.
[40] V.V. Atuchin, I.E. Kalabin, V.G. Kesler, N.V. Pervukhina, J. Electron Spectrosc. Relat. Phenom. 142 (2005) 129.
[41] S.L.T. Anderson, J. Chem. Soc., Faraday Trans. 75 (1979) 1356.
[42] L.Z. Zhao, S.H. Lui, D.H. Wang, C.H. Pan, J. Electron Spectrosc. Relat. Phenom. 52 (1990) 571.
[43] D.C. Phillips, S.J. Sawhill, R. Self, M.E. Bussell, J. Catal. 207 (2002) 266.
[44] O.A. Balitskii, W. Jaegermann, Mater. Chem. Phys. 97 (2006) 98.
[45] P. Forzatti, F. Trifiró, P.L. Villa, J. Catal. 55 (1978) 52.
[46] G. Centi, F. Trifiró, Appl. Catal. 12 (1984) 1.
[47] M. Baca, A. Pigamo, J.L. Dubois, J.M.M. Millet, Catal. Commun. 6 (2005) 215.
[48] D. Vitry, Y. Morikawa, J.L. Dubois, W. Ueda, Appl. Catal. A 251 (2003) 411.
[49] P. Botella, P. Concepción, J.M. López Nieto, Y. Moreno, Catal. Today 99 (2005) 51.
[50] D. Vitry, Y. Morikawa, J.L. Dubois, W. Ueda, Top. Catal. 23 (2003) 47.
[51] F. Smet, P. Ruiz, B. Delmon, M. Devillers, J. Phys. Chem. B 105 (2001) 12355.
[52] M. Baca, A. Pigamo, J.L. Dubois, J.M.M. Millet, Top. Catal. 23 (2003) 39.
[53] L.T. Weng, B. Delmon, Appl. Catal. A 81 (1992) 141.
[54] F. Barbieri, D. Cauzzi, F. De Smet, M. Deviller, P. Moggi, G. Predieri, P. Ruiz, Catal. Today 61 (2000) 353.
[55] E.M. Gaigneaux, H. Liu, H. Imoto, T. Shido, Y. Iwasawa, Top. Catal. 11–12 (2000) 185.
[56] P. Botella, J.M. López Nieto, B. Solsona, J. Mol. Catal. A 184 (2002) 335.
[57] T.V. Andrushkevich, G.K. Boreskov, L.L. Kuznetsova, L.M. Plyasova, Yu.N. Tyurin, Yu.M. Schekochikhin, Kinet. Catal. 15 (1974) 369.
[58] H. Hibst, F. Rosowski, G. Cox, Catal. Today 117 (2006) 234.
[59] G. Mestl, T. Ilkenhans, D. Spielbauer, M. Dieterle, O. Timpe, H.J. Krohnert, F. Jentoff, H. Knözinger, R. Schlögl, Appl. Catal. A: Gen. 210 (2001) 13.
[60] G. Mestl, Top. Catal. 38 (2006) 69. and references therein.
[61] R.K. Grasselli, C.G. Lugmair, A.F. Volpe, A. Andersson, J.D. Burrington, Catal. Lett. 126 (2008) 231.